Macroscopic resonant tunneling in an rf-SQUID flux qubit*

Cong Shan-Hua(丛山桦)[a], Wang Yi-Wen(王轶文)[b], Sun Guo-Zhu(孙国柱)[a]†, Chen Jian(陈 健)[a], Yu Yang(于 扬)[b], and Wu Pei-Heng(吴培亨)[a]

[a] *Research Institute of Superconductor Electronics, School of Electronic Science and Engineering, Nanjing University, Nanjing* 210093, *China*

[b] *National Laboratory of Solid State Microstructures, School of Physics, Nanjing University, Nanjing* 210093, *China*

(Received 8 October 2010; revised manuscript received 10 December 2010)

We have observed the macroscopic resonant tunneling of magnetic flux between macroscopically distinct quantum states in a superconducting flux qubit. The dependences of the macroscopic resonant tunneling on the barrier height of the potential well, the flux bias and the initial state are investigated. Detailed measurements of the tunneling rate as a function of the flux bias reveal the feature of the quantum noise in the superconducting flux qubit.

Keywords: rf-SQUID, macroscopic resonant tunneling, quantum noise, flux qubit

PACS: 03.75.Lm, 85.25.Dq, 03.67.Lx, 42.50.Lc **DOI:** 10.1088/1674-1056/20/5/050316

1. Introduction

Superconducting qubits have aroused a lot of interest because of the fundamental quantum physics and the promising application in the quantum information processing.[1,2] While more and more striking progress has been achieved in the past decades, more and more difficulties have appeared on the road to the implementation of quantum processing. For instance, the performance of the qubits is limited by the short energy relaxation time and dephasing time, which may result from the designs, circuits and materials.[3−8] Recently, Harris *et al.*[9] reported the observation of the quantum mechanical low frequency noise with $1/f$ frequency dependence, which led to the shift of Gaussian shaped resonant tunneling rate. In the present article, we use another method to present our measurements of the quantum noise in the radio frequency superconducting quantum interference device (rf-SQUID) flux qubit. Instead of measuring the tunneling delay time directly, we extract the tunneling rate from the relationship between probability and the flux bias, with the initial state prepared.

An rf-SQUID flux qubit is generally composed of a superconducting loop with inductance L interrupted by a Josephson junction with capacitance C and critical current $I_{\rm c}$. The dynamics of the rf-SQUID can be described in terms of a variable Φ and is identical to that of a particle of 'mass' C moving in a potential well

$$U(\Phi) = U_0 \left[\frac{1}{2} \left(\frac{2\pi(\Phi - \Phi_{\rm f}^{\rm q})}{\Phi_0} \right)^2 - \beta_{\rm L} \cos\left(\frac{2\pi\Phi}{\Phi_0} \right) \right], \tag{1}$$

where $\Phi_0 \equiv h/2e$ is the flux quantum, $U_0 = \Phi_0^2/(4\pi^2 L)$, and $\beta_{\rm L} = 2\pi L I_{\rm c}/\Phi_0$. For a proper $\beta_{\rm L}$, when magnetic flux $\Phi_{\rm f}^{\rm q}$ close to $\Phi_0/2$ is applied, the system has a double potential well. Energy levels localized in different wells represent different flux states, which correspond to macroscopic currents circulating around the loop in the clockwise and the anticlockwise directions. Flux can tunnel between the opposite wells when the energy levels in the two wells are aligned,[10] generating a change of the circulating current direction, which can be discriminated by a dc-SQUID magnetometer.

2. Model and method

Our samples are fabricated with $\rm Nb/AlO_{\it x}/Nb$ trilayer on an oxidized Si wafer using a standard photolithography process. A schematic layout of one of

*Project supported by the New Century Excellent Talents in University, China, the National Natural Science Foundation of China (Grant Nos. 11074114 and 10874074), and the National Basic Research Program of China (Grant No. 2011CBA00200).

†Corresponding author. E-mail: gzsun@nju.edu.cn

© 2011 Chinese Physical Society and IOP Publishing Ltd

the samples is shown in Fig. 1. The qubit is essentially an rf-SQUID in the second order gradiometric design.[11] Two tunnel junctions in parallel named compound Josephson junctions (CJJs) are used instead of one in order to adjust I_c with an applied dc flux bias Φ_f^{CJJ}, which consequently changes the barrier height of the well *in situ*. We use an on-chip flux bias line to control the tilt of the potential with an applied dc flux bias Φ_f^q. Additional flux bias line is used to produce Φ_f^{dc}, thus biasing the readout dc-SQUID at the maximum sensitivity region. The mutual inductance between the qubit and dc-SQUID is well designed so that we can distinguish the different fluxes generated by the circulating currents in the qubit. The sample is mounted on a chip carrier enclosed in a superconducting aluminum sample cell. The assembly is thermally anchored to the mixing chamber of dilution refrigerator with base temperature $T = 20$ mK and magnetically shielded by three layers of Mu-metal cylinders surrounding the Dewar bottle at room temperature. All electrical leads that connect the junction to room temperature electronics are carefully filtered by RC filters and copper-powder filters. Battery-powered low-noise pre-amplifiers are used for all measurements. All the on-chip flux bias lines mentioned above are inductively coupled to the qubit. A 20 dB attenuator at 1 K stage and a 10 dB attenuator at 20 mK stage are used to reduce the external noise along the current bias circuit.

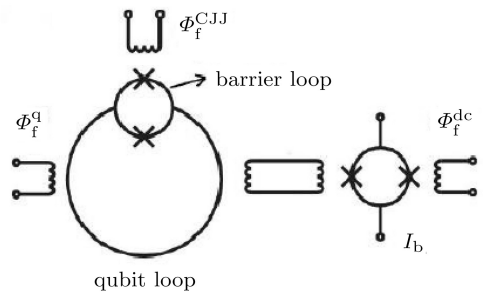


Fig. 1. Schematic of the sample layout, where the crosses represent Josephson junctions and Φ_f^{dc}, Φ_f^{CJJ} and Φ_f^q denote the flux bias for the dc-SQUID, compound Josephson junctions and qubit, respectively.

There are several methods to measure the macroscopic resonant tunneling (MRT) in the rf-SQUID qubit.[9,11,12] The time profile of the measurement sequence in our experiments is shown in Fig.2. Having calibrated the sample parameters, we set the flux bias Φ_f^{CJJ}, with which the potential barrier between the wells is not too high for the experiments. Beside Φ_f^q, which determines the energy levels in the wells, an additional short pulse is added to the qubit in order to prepare the initial state in one of the wells. After shutting down the preparing flux pulse and waiting for a delay time t_{delay}, a readout current pulse with a rising time of 5 ns is applied to dc-SQUID. By setting the amplitude and the duration of readout current pulse properly, we can observe that dc-SQUID either switches to a finite voltage or stays at zero voltage, corresponding to the qubit state in the left well $|L\rangle$ or in the right well $|R\rangle$. The switching probability can be obtained by repeating the trials 5000 times, thereby representing the probability of the qubit being in $|R\rangle$ state. Then we change Φ_f^q gradually, repeat the above measurement and obtain the population as a function of Φ_f^q.

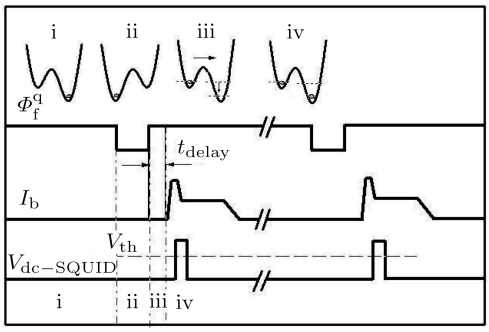


Fig. 2. Time profile of the measurement sequence, where the upper insets illustrate the changes of the potential wells.

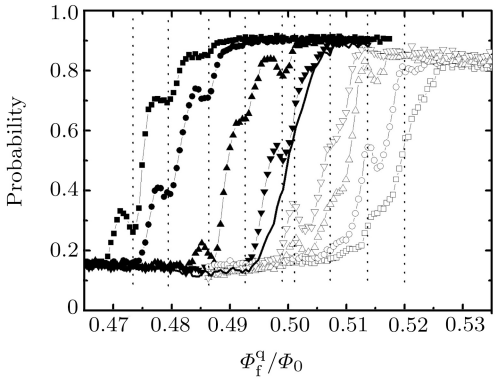


Fig. 3. Curves for probability versus Φ_f^q with the initial state prepared in one of the double wells, where dotted lines indicate the locations where the lowest energy levels in one well cross the energy levels in the opposite well.

Figure 3 shows the typical data of the probability being in $|R\rangle$ as a function of the flux bias. The solid line represents the measured probability without the initial state prepared. As expected, it is symmetric about $\Phi_f^q = 0.5\Phi_0$. The curve to the left of the solid line is the probability measured when the initial state

is prepared in the left well. The dips indicated by the dotted lines correspond to the lowest energy levels in the left well crossing successively the different levels in the right well, generating a maximum transition rate from the left to the right well. For the curve to the right of the solid line, the initial state is prepared in the right well. Similarly, peaks can be observed at the flux bias where the levels between two wells are lining up and generating maximum transition to the left well. These curves have different values of $t_{\rm delay}$. The closer curves to the solid line correspond to the longer $t_{\rm delay}$.

3. Discussion

In order to compare our experiment with the theory quantitatively, we extract the tunneling rates at different flux bias. From the master equations, we have

$$\begin{cases} \dfrac{{\rm d}P_{\rm L}}{{\rm d}t} = -\Gamma_{\rm LR}P_{\rm L} + \Gamma_{\rm RL}P_{\rm R}, \\ P_{\rm L} + P_{\rm R} = 1, \\ \dfrac{\Gamma_{\rm LR}}{\Gamma_{\rm RL}} = {\rm e}^{\varepsilon/T_{\rm eff}}, \end{cases} \tag{2}$$

where $P_{\rm L}$ and $P_{\rm R}$ are the populations in $|L\rangle$ and $|R\rangle$ respectively, $\Gamma_{\rm LR}$ and $\Gamma_{\rm RL}$ are the rates of tunneling transitions between the two wells, ε is the bias energy between the wells and $T_{\rm eff}$ is the effective temperature. By solving Eq. (1), we obtain $P_{\rm L}$ as a function of t,

$$P_{\rm L} = C_1 \cdot {\rm e}^{-(1+{\rm e}^{-A})\Gamma_{\rm LR}t} + \frac{1}{1+{\rm e}^{A}}, \tag{3}$$

where $A = \dfrac{\varepsilon}{T_{\rm eff}}$ and C_1 is a constant.

Therefore, for each $\Phi_{\rm f}^{\rm q}$, we measure the probability of being in $|R\rangle$ state as a function of $t_{\rm delay}$. Shown in Fig. 4 is an example of the probability versus $t_{\rm delay}$. By fitting it using Eq. (3) we obtain the tunneling rate Γ. Then we reset $\Phi_{\rm f}^{\rm q}$, repeat the procedure. We obtain Γ as a function of $\Phi_{\rm f}^{\rm q}$, which is shown in Fig. 5. The squares and the circles represent the tunneling rates with the initial state prepared in the different wells. They are symmetric about $0.5\Phi_0$. When the levels in different potential wells cross each other, the tunneling rates are enhanced due to the maximizing of the density states. The inset of Fig. 5 shows that at $0.5\Phi_0$, the Gaussian-shape tunneling rate peak splits into two peaks. According to Ref. [13], in the presence of low frequency flux noise, the transition rate $\Gamma_{\rm LR}$ is found to be

$$\Gamma_{\rm LR} = \sqrt{\frac{\pi}{8}}\frac{\Delta^2}{W}\exp\Big[-\frac{(\varepsilon-\varepsilon_{\rm p})^2}{2W^2}\Big],$$

in which Δ, W and $\varepsilon_{\rm p}$ represent the tunneling amplitude, the width of the tunneling rate and the energy shift, respectively. For a classical noise, $\varepsilon_{\rm p} = 0$, so the tunneling rate is symmetric about $0.5\Phi_0$; yet for a quantum noise, $\varepsilon_{\rm p} \neq 0$, so the tunneling rate is shifted and the peak symmetric about $0.5\Phi_0$ splits into two peaks. This is a signature of the presence of the strong low frequency noise.[9] Considering the large geometrical size of our sample, the splitting is reasonable.

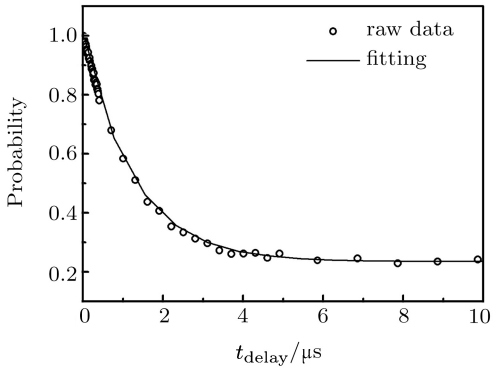


Fig. 4. Probability versus $t_{\rm delay}$ at $\Phi_{\rm f}^{\rm q}$, from which we can obtain the tunneling rate by fitting with the theoretical model.

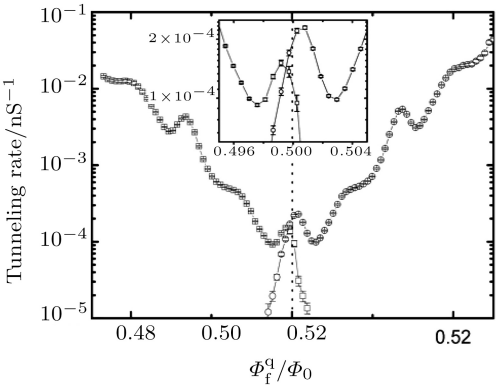


Fig. 5. Tunneling rate versus $\Phi_{\rm f}^{\rm q}$. The inset clearly shows the splitting of the tunneling rate peak around $0.5\Phi_0$, which is caused by the quantum noise in the qubit.

It is interesting to notice that though around each crossing point, the tunneling rate is enhanced because the energy levels in the double well align with each other, but is not always a maximum (Fig. 5). The relative peak height of the tunneling rate at the crossing point seems to be periodically modulated as a function of $\Phi_{\rm f}^{\rm q}$. This is counterintuitive and also observed when we change the barrier height of the qubit. Further experiments are needed to clarify whether it is intrinsic or artificial.

4. Conclusion

Using a fast readout pulse, we have measured the probabilities and tunneling rate each as a function of the flux bias in the rf-SQUID flux qubit by preparing the initial state in one of the double wells. Peaks and dips due to the resonant tunneling are observed when the levels in opposite wells line up. The quantum noise in the qubit leads to the splitting of the middle resonant tunneling peak.

Acknowledgement

We are grateful to J. E. Lukens *et al.* for the samples.

References

[1] Makhlin Y, Schön G and Shnirman A 2001 *Rev. Mod. Phys.* **73** 357

[2] Clarke J and Wilhelm F K 2008 *Nature* **453** 1031

[3] Astafiev O, Pashkin Y A, Nakamura Y, Yamamoto T and Tsai J S 2004 *Phys. Rev. Lett.* **93** 267007

[4] Yoshihara F, Harrabi K, Niskanen A O, Nakamura Y and Tsai J S 2006 *Phys. Rev. Lett.* **97** 167001

[5] Bialczak R C, McDermott R, Ansmann M, Hofheinz M, Katz N, Lucero E, Neeley M, O'Connell A D, Wang H, Cleland A N and Martinis J 2007 *Phys. Rev. Lett.* **99** 187006

[6] Yu Y, Zhu S, Sun G Z, Wen X D, Dong N, Chen J, Wu P H and Han S Y 2008 *Phys. Rev. Lett.* **101** 157001

[7] Lanting T, Berkley A J, Bumble B, Bunyk P, Fung A, Johansson J, Kaul A, Kleinsasser A, Ladizinsky E, Maibaum F, Harris R, Johnson M W, Tolkacheva E and Amin M H S 2009 *Phys. Rev.* B. **79** 060509

[8] McDermott R 2009 *IEEE. Trans. Appl. Supercond.* **19** 2

[9] Harris R, Johnson M W, Han S Y, Berkley A J, Johansson J, Bunyk P, Ladizinsky E, Govorkov S, Thom M C, Uchaikin S, Bumble B, Fung A, Kaul A, Kleinsasser A, Amin M H and Averin D V 2008 *Phys. Rev. Lett.* **101** 117003

[10] Lu W T, Wang S J and Zhang H 2010 *Chin. Phys.* B **19** 020304

[11] Sun G Z, Wen X D, Wang Y W, Cong S H, Chen J, Kang L, Xu W W, Yu Y, Han S Y and Wu P H 2009 *Appl. Phys. Lett.* **94** 102502

[12] Bennett D A, Longobardi L, Patel V, Chen W and Lukens J E 2007 *Supercond. Sci. Technol.* **20** S445

[13] Amin M H S and Averin D V 2008 *Phys. Rev. Lett.* **100** 19700